# Digital Signal Processing for Coherent Optical Communication

Xiang Zhou
AT&T Labs-Research, Middletown NJ, 07748, USA
Email: zhoux@research.att.com

Jianjun Yu
NEC Laboratories America, Princeton, NJ 08540, USA
Email: Jianjun@nec-labs.com

***Abstract*** — In this paper we review several digital signal processing (DSP) algorithms recently proposed (or introduced) for coherent optical communication system. There include the digital equalization algorithms for chromatic dispersion (CD) compensation, polarization recovery, and polarization mode dispersion compensation (PMD), and DSP algorithms for carrier frequency offset estimation and carrier phase recovery. A novel distortion mitigation algorithm developed for coherent receiver using single-ended photodetection will also be discussed.

**Keywords-DSP, Coherent, algorithm, optical, detection, communication**

## I. INTRODUCTION

Digital signal processing (DSP) based coherent detection technology is revolutionizing optical communication. This technology moves the complexity of phase and polarization tracking into the digital domain, which not only simplifies the reception of various multi-level, multi-dimensional-coded optical signals, it also enables several major optical impairments (CD, PMD and optical filtering effects) being compensated in the digital domain. As a result, DSP-based digital coherent detection (combined with multilevel, multidimensional coding) has emerged as a promising method for achieving higher data rate and higher SE, and therefore is a very active research topic [1-16].

In this paper we review several DSP algorithms recently proposed (or introduced) for coherent optical communication system. These include the digital equalization algorithms for polarization recovery, CD and PMD compensation, the DSP algorithms for carrier frequency and phase recovery as well as a new distortion mitigation algorithm developed for coherent receiver using single-ended photodetection.

## II. DSP ALGORTIHMS FOR A TYPICAL DIGITAL COHERENT RECIVER

For a typical digital coherent receiver, the incoming optical field is coherently mixed with a local oscillator (LO) through a polarization- and phase-diverse 90 ° hybrid. This hybrid separates the in-phase and quadrature components of the received optical field in both X- and Y-polarizations, which can then be detected using either four balanced photodetectors or four single-ended photodetectors using a high LO-to-signal power ratio. The detected analog electrical signals are digitized by four analog-to-digital converters (ADCs) and then go to a digital signal processing (DSP) unit, which is the heart of a digital coherent receiver. In Fig. 1 we show an illustration of a digital coherent receiver using single-ended photo detection with the typical DSP functional blocks included. The DSP part consists of two 'fixed' digital equalizers, four butterfly-configured adaptive digital equalizers, and carrier-frequency- and phase-recovery units. Clock recovery and soft decision may also be implemented with DSP.

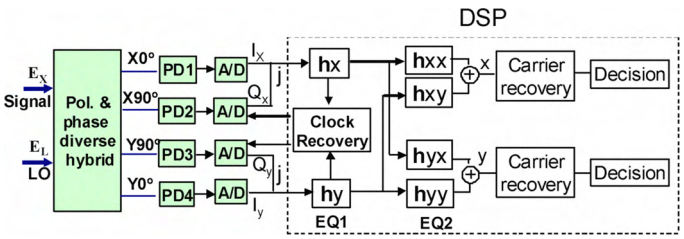


Fig. 1. Illustration of a typical digital coherent receiver using single-ended photo detection, PD: photodetector, EQ: equalizer

The two 'fixed' (or slowly adaptable) equalizers (EQ1 in Fig. 1) are used for digital compensation of large amounts of CD for an optical transmission system without optical dispersion compensation. In most of the recently demonstrated coherent transmission experiments, a T/2-spaced time-domain finite impulse response (FIR) filter was employed to achieve the best performance. However, to reduce receiver complexity, 2T/3-spaced (sample rate=1.5×symbol rate) equalization may be used, because 1.5×symbol rate is already greater than the double-side receiver bandwidth (i.e. the Nyquist frequency). The required filter coefficients can be obtained from the (approximately) known fiber CD transfer function using either the frequency-domain truncation method or the time-domain truncation method [1]. It has been shown that time-domain truncation requires fewer filter taps than frequency-domain truncation. But even with time-domain truncation, more than 250 T/2-spaced filter taps are still required for a 28Gbaud system for 1000km transmission distance over standard single mode fiber (SSMF) [1]. To reduce the complexity of CD compensation, fast Fourier transform (FFT)-based frequency-domain equalization (FDE) has recently been introduced for CD compensation [2]. Unlike the time-domain FIR filter whose computation complexity scales with the square of the symbol rate, the computation complexity of FDE increases with symbol rate only on a log

978-1-4244-5217-0/09/$25.00 ©2009 IEEE

scale. As a result, FDE may be a more practical method for high-speed coherent communication systems.

The four adaptive digital equalizers (EQ2 in Fig. 1) are used for polarization recovery and de-multiplexing, polarization-mode-dispersion (PMD) compensation as well as residual CD compensation. Other linear distortions such as optical filtering effects can also be compensated by this adaptive equalization. T/2–spaced time-domain FIR filters are commonly used as the equalizers to achieve the best performance. As discussed above, a 2T/3-spaced equalizer may also be used to reduce receiver complexity. For 2T/3 equalization, the filter coefficients are updated twice for every three samples, so an extra interpolator is required to obtain the second T-spaced samples. The filter coefficients are typically updated by using a constant modulus algorithm (CMA) [17] or by initializing with CMA for pre-convergence and then switching to a decision-directed least-mean square (LMS) algorithm once stable operation is achieved. A detailed description of the tap coefficient update procedure using CMA and LMS can be found in [1].

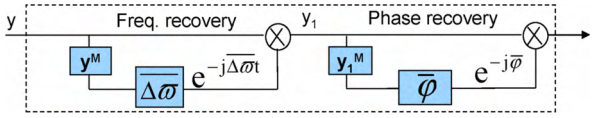


Fig. 1. Illustration of Mth-power based carrier recovery

There are two typical methods for carrier frequency estimation and phase recovery. The first is the Mth-power feed-forward method (i.e. the Viterbi-Viterbi method) [18]. For this method, the signal is first raised to Mth-power to remove the data modulation (M=4 for QPSK, M=8 for 8PSK) and then the frequency offset between the transmitted signal and the LO is decided from the speed of the phase rotation of the resulting signal [16]. After removing the frequency offset, the frequency-recovered signal is raised to Mth-power again to remove the data modulation. Because the laser phase noise changes more slowly than the other received noise contributions such as amplified spontaneous emission (ASE) noise, the phase noise can be estimated by averaging over multiple adjacent symbols. Fig. 10 is an illustration of the Mth-power-based carrier recovery algorithm. The alternate carrier recovery method uses maximum-likelihood (ML) estimation [19]. ML estimation is based on the assumption that the laser phase $\psi$ does not change over multiple symbol periods. Over this period of time, the ML estimate of $\psi$ is the value that maximizes $P(r|\psi)$, the probability density function (PDF) of the received signal $r$ conditioned on $\psi$. Assuming white and zero-mean Gaussian noise, the ML estimate of $\psi$ can be expressed as [19]

$$\hat{\psi}_{ML} = -\tan\left[\mathrm{Im}\left(\sum_{n=0}^{K-1} I_n^* r_n\right) \Big/ \mathrm{Re}\left(\sum_{n=0}^{K-1} I_n^* r_n\right)\right] \qquad (1)$$

where K denotes the number of symbols over which $\psi$ does not change, and $I$ is the correctly detected signal. Because correct decision is required, ML estimation only works in a decision-directed or decision feedback mode.

## III. DISTORTION MITIGATION ALGORITHM

A digital coherent receiver using single-ended photodetection may have a significant cost advantage compared to a coherent receiver using balanced detection. But this cost advantage comes with a problem that the direct square-law detection of the modulated signal will cause distortion to the original signal. Such distortion may severely degrade the performance of DSP-based dispersion compensation, polarization recovery, and PMD compensation, especially for high-level modulated optical signals. Traditionally, this distortion is mitigated using very large LO-to-signal power ratio (LOSPR) [8]. We recently reported a DSP-based method to address this problem [13]. The method allows single-ended photodetection to be used with significantly lower LOSPR. A lower LOSPR will relax the requirement on LO power and RIN, and therefore should ease the design of a coherent receiver.

For a polarization- and phase-diverse coherent receiver using single-ended photodetection, the signal powers eceived by the photodetector (PD) in the in-phase (0°) and quadrature branch (90°) at one of the two polarizations are given by

$$P_I(t) = P_S(t) + P_L(t) + 2\sqrt{P_S(t)P_L(t)}\cos(\theta(t)) \qquad (2)$$

$$P_Q(t) = P_S(t) + P_L(t) + 2\sqrt{P_S(t)P_L(t)}\sin(\theta(t)) \qquad (3)$$

Here $P_S(t)$ and $P_L(t)$ denote the signal and LO power, respectively. $\theta(t)$ represents the relative phase between the received optical signal and the reference optical signal (i.e. the LO). After photodetection and A-to-D conversion, the digitized electrical signal with AC coupling can be approximated as

$$I_I(n) \approx \tilde{I}_S(n) + 2\sqrt{I_S(n)I_L(n)}\cos(\theta(t_n)) \qquad (4)$$

$$I_Q(n) \approx \tilde{I}_S(n) + 2\sqrt{I_S(n)I_L(n)}\sin(\theta(t_n)) \qquad (5)$$

where $I_S(n)$ and $I_L(n)$ denote the photodetected signal and LO at the n$^{th}$ sampling time, respectively. $\tilde{I}_S(n)$ is the AC component of $I_S(n)$. To obtain (4) and (5) we have assumed that, 1) the LO intensity noise (i.e. the AC component of $I_L(n)$) is very small and negligible, and 2) the electrical bandwidth at the receiver is greater than (or close to) the signal bandwidth. The purpose of the proposed DSP algorithm is to find the approximate value of $\tilde{I}_S(n)$. Assume that $I_L(n) >> I_S(n)$, then to a first-order approximation we can have

$$I_I(n) \approx 2\sqrt{I_S(n)I_L(n)}\cos(\theta(t_n)) \qquad (6)$$

$$I_Q(n) \approx 2\sqrt{I_S(n)I_L(n)}\sin(\theta(t_n)) \qquad (7)$$

Note that we can write $I_S(n)$ and $I_L(n)$ in (6) and (7) as

$$I_S(n) = \bar{I}_S(n) + \tilde{I}_S(n) \qquad (8)$$

$$I_L \approx \bar{I}_L \qquad (9)$$

where the bar over the symbols denotes the DC component (i.e. time-averaged portion). From (6)-(9), we find

$$I_I^2(n)+I_Q^2(n)\approx 4\tilde{I}_S(n)\bar{I}_L(n)+4\bar{I}_S\bar{I}_L \quad (10)$$

$$\overline{I_I^2+I_Q^2}=4\bar{I}_S\bar{I}_L \quad (11)$$

Using (10) and (11), the first-order approximation for $\tilde{I}_S(n)$ is

$$\tilde{I}_S^{(1)}(n)=\frac{I_I^2(n)+I_Q^2(n)-\overline{I_I^2+I_Q^2}}{4\bar{I}_L} \quad (12)$$

Note that $\bar{I}_L$ is a constant that only depends on the LO power and the receiver configuration. Its value can be determined easily by doing an initial calibration. For a typical coherent communication system with sampling rate equal to twice the baud, the known LOSPR (defined as $\bar{P}_L/\bar{P}_S$) can be approximated as $\bar{I}_L/\bar{I}_S$. Thus $\bar{I}_L$ can be deduced from $I_I(n)$, $I_Q(n)$ and LOSPR as

$$\bar{I}_L\approx 0.5\sqrt{\overline{I_I^2+I_Q^2}\cdot \mathrm{LOSPR}} \quad (13)$$

To find the second-order approximation for $\tilde{I}_S(n)$, we can simply replace $I_I(n)$ and $I_Q(n)$ in Eq. (6) and (7) by $I_I(n)-\tilde{I}_S^{(1)}(n)$ and $I_Q(n)-\tilde{I}_S^{(1)}(n)$, thus we have

$$\tilde{I}_S^{(2)}(n)=\frac{\left\{I_I(n)-\tilde{I}_S^{(1)}(n)\right\}^2+\left\{I_Q(n)-\tilde{I}_S^{(1)}(n)\right\}^2}{4\bar{I}_L}-\frac{\overline{\left\{I_I(n)-\tilde{I}_S^{(1)}(n)\right\}^2+\left\{I_Q(n)-\tilde{I}_S^{(1)}(n)\right\}^2}}{4\bar{I}_L} \quad (14)$$

If a refined $\bar{I}_L$ is to be calculated using Eq. (13), $I_I(n)$ and $I_Q(n)$ in Eq. (13) also need to be replaced by $I_I(n)-\tilde{I}_S^{(1)}(n)$ and $I_Q(n)-\tilde{I}_S^{(1)}(n)$, respectively. A similar method can be used to obtain a higher-order approximation for $\tilde{I}_S(n)$.

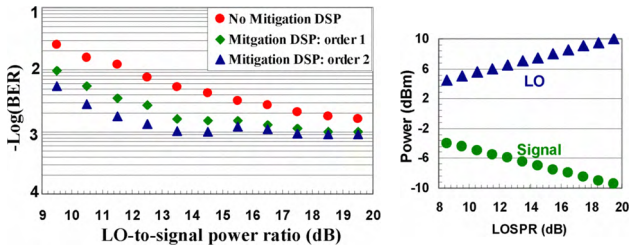


(a) (b)

Fig. 2(a) Measured BER versus LOSPR with different processing scenarios and (b) average signal and LO power incident on the PDs versus LOSPR

The algorithm described in Eqs. 12 to 14 has been tested in an 8 ×114 Gb/s, 25GHz-spaced DWDM transmission experiment using return-to-zero (RZ) pulse-shaped PDM-8PSK modulation (experimental setup is described in [10]). For this experiment, the launch power was chosen to be -2.5 dBm and the received optical signal-to-noise ratio (OSNR) of ch. 4 after 640 km transmission was 25 dB (in 0.1 nm noise bandwidth). Fig. 11(a) shows the measured BER of channel 4 versus various values of LOSPR after 640km of transmission with three different post-processing scenarios: (1) without using the proposed DSP algorithm, 2) using the proposed algorithm with for a first-order approximation, and (3) using the proposed algorithm with an approximation up to second order. Different values of LOSPR were obtained by changing both the signal and LO power in a way that the effective power from the coherent-mixing term remained constant. That way the penalty from the sampling scope due to its noise floor and limited ADC resolution (5.5 effective bits) does not change with LOSPR. With the signal and LO powers shown in Fig. 2(b), the estimated shot noise and thermal noise are small compared to the LO-ASE beat noise. Thus the received electrical SNR before the sampling scope can be approximated as

$$SNR\approx\frac{\bar{P}_L\cdot OSNR\cdot B_O}{(\bar{P}_s+\bar{P}_L)B_e} \quad (15)$$

where $B_e$ denotes the electrical bandwidth, and $B_O$ denotes the optical noise bandwidth used for OSNR measurement. Note that with a constant OSNR, and $\bar{P}_L>>\bar{P}_S$, SNR does not change with LOSPR. Thus the performance difference between different values of LOSPR shown in Fig. 2(a) mainly comes from the distortion caused by $\tilde{I}_S(n)$. With LOSPR varying from 9.5 dB to 19.5 dB, the best BER achieved using the traditional method is $1.6\times10^{-3}$ at LOSPR of 19.5 dB. By using a second-order approximation, however, the proposed algorithm allows a similar performance to be achieved with LOSPR of 11.5 dB. At the same LOSPR of 19.5 dB, the proposed algorithm improved the BER from $1.6\times10^{-3}$ to $9\times10^{-4}$. For the proposed algorithm, the performance for approximations with orders higher than 2 was also investigated, and we found that the performance difference between second and higher orders is small. With the proposed algorithm, our simulation also shows that a digital coherent receiver using single-ended photodetection can achieve similar performance as a receiver using balanced detection, without using a very high LOSPR.

## IV. CASCADED MULTI-MODULOUS EQUALIZATION ALGORITHM

The classic CMA has been shown to be very effective for blind polarization de-multiplexing of PDM-QPSK and PDM-8PSK signals. It has been shown that CMA-based blind equalization can achieve a performance close to decision-directed LMS (DD-LMS) [1] and therefore can be used as a stand-alone equalization algorithm (the performance of DD-LMS depends on error rate and may fail with long error bursts).

For PDM-8QAM and 16QAM, however, it is found that the classic CMA algorithm is no longer effective as a stand alone equalization algorithm [14,20]. This is because an 8QAM or 16QAM signal does not present constant symbol amplitude. As a result, the CMA error signal will not approach zero even for an ideal 8-QAM or 16-QAM signal,

resulting in extra noise after equalization. To address this issue, we recently proposed a new cascaded multi-modulus algorithm (CMMA) [14]. The principle of the proposed new algorithm in terms of the error signal calculation method for 8QAM is illustrated in Fig. 3, where we show an ideal circular 8-QAM signal, the equation for error signal calculation, and the calculated intermediate and final errors. For this algorithm, two reference circles with modulus of $(R1+R2)/2$ and $(R1-R2)/2$ are introduced in a cascaded way such that the final error signal will approach zero for an ideal 8QAM signal. Note that R1 and R2 denote the radius of the two circles where the 8QAM constellation points are located. For comparison, the error signal for the classic CMA is calculated using only one reference circle with a constant modulus of $E|Z|^2/E|Z|$ [17]. It is clear that for PDM-8QAM and PDM-16QAM the CMA cannot have zero error even after perfect equalization.

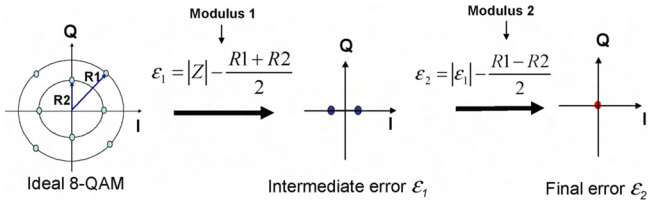


Fig. 3. Illustration of the proposed algorithm for PDM-8QAM signals

The CMMA has been experimentally verified in a 60-Gb/s PDM-8QAM experiment. The experimental setup is shown in Fig. 4a. The details of the 8QAM modulator are shown in Fig. 4. It consisted of a commercial dual- parallel MZM with a 3 dB bandwidth of about 15GHz and a phase modulator with a 3 dB bandwidth greater than 30GHz. The 8QAM modulator was driven by three 10-Gb/s $2^{11}$-1 PRBS binary signals. The generated 8-QAM signal was then divided and recombined with about 1.6ns time delay by using a polarization beam combiner (PBC) to generate the required PDM-8QAM signal. At the receiver, amplified spontaneous emission (ASE) noise was added by attenuating the signal before an optical amplifier. The amplified signal passed through a 0.3 nm optical filter and then was mixed with a local oscillator (LO) signal in a polarization and phase-diverse hybrid. A narrow linewidth (~100kHz) external cavity laser (ECL) was used for both the LO and the signal source. The frequency of the LO was tuned within 500 MHz of the transmit laser. At the output of the optical hybrid four single-ended photodetectors were used to convert the optical signals into electrical signals. The sampling and digitization (A/D) function was achieved with a 4-channel real-time sampling scope (50 Gsa/s, 18-GHz electrical bandwidth and 5.5 bit effective resolution). The captured data was then post-processed using a desktop PC.

This experiment's digital signal processing consisted of six steps. First the baud clock was extracted by using the classic "square and filter" method. Second, the 50 Gsa/s signal was down-sampled to a sample rate of twice the baud using the extracted clock (an anti-aliasing filter is used before re-sampling). Third, the distortion from direct square-law detection of the signal component due to single-ended photo-detection was mitigated using the algorithm described above (Section III. B). Next, polarization de-multiplexing was performed with four 13-tap, T/2-spaced adaptive FIR filters, optimized by the above-described CMMA. Carrier frequency and phase recovery were performed in the subsequent step using a feed-forward M-th power algorithm [18]. Finally, differential decoding, Gray-code mapping and BER counting were done. For all reported results, BERs were counted over $2.4\times10^6$ bits.

Without added ASE noise, the measured electrical eye diagram (through direct detection) and the constellation diagram of the generated 30-Gb/s 8QAM signal are shown in Fig. 4b and Fig. 4c, respectively. After noise loading, the measured BER versus OSNR (0.1 nm noise BW) for both the single polarization 8QAM signal and the PDM-8QAM signal are shown in Fig. 5a. The required OSNR to achieve $2\times10^{-3}$ BER for single polarization 30-Gb/s 8-QAM and 60-Gb/s PDM-8QAM are 13.4 and 16.4 dB, respectively. No excess PDM penalty was observed when using the proposed polarization de-multiplexing algorithm. For comparison, Fig. 5b shows the recovered constellation diagrams obtained from the proposed new CMMA and from the classic CMA, for a 60-Gb/s PDM-8QAM signal at OSNR of 17.1 dB, where X and Y denote the two orthogonal polarizations. It is clear that the classic CMA is not effective for an 8QAM signal.

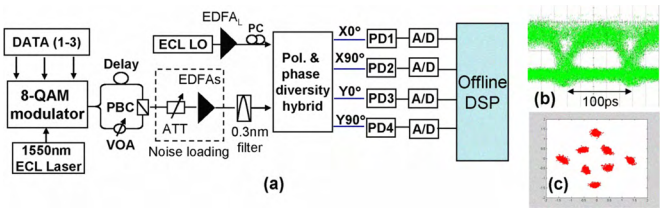


Fig. 4 (a) Experimental setup, (b) the measured electrical eye diagram and (c) the constellation diagram of the generated 30-Gb/s 8-QAM signal.

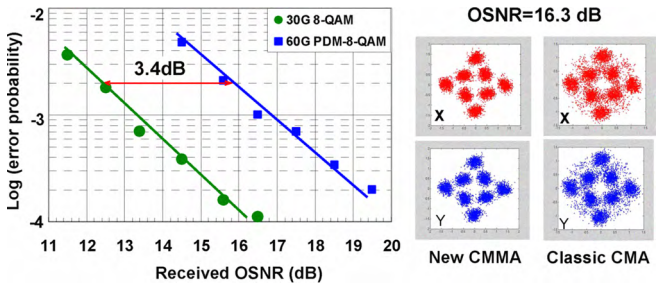


Fig. 5. (a) Measured BER versus OSNR for 30Gb/s and 60Gb/s PDM-8QAM, (b) recovered constellation diagrams using two algorithms

Using a similar experimental setup to that shown in Fig. 4a, we successfully generated and detected a 114 Gb/s PDM-8QAM optical signal using an 8QAM modulator with higher bandwidth.

We should also mention that a different multi-modulus algorithm has recently been proposed for PDM-16QAM

[20].This algorithm relies on a pre-decision to decide which modulus should be used for error signal calculation. For both the cascaded multi-modulus algorithm and the pre-decision assisted multi-modulus algorithm, more work needs to be done to understand their convergence performance under various polarization-mixing conditions.

## V. Conclusions

Digital signal processing algorithms for chromatic dispersion (CD) compensation, polarization recovery, polarization mode dispersion compensation (PMD) and carrier recovery have been discussed. It is shown that while both time-domain and frequency-domain equalization can be used for CD compensation, time-domain based equalization algorithms require much more computational efforts than the frequency-domain based equalization algorithm. For adaptive polarization recovery, it is shown that the widely used constant-modulus algorithm is no longer effective as a standalone equalization algorithm for modulation formats without presenting constant amplitude. We then give a detailed description on a recently proposed cascaded multi-modulus algorithm for blind polarization de-multiplexing of PDM-8QAM signal. In addition to DSP algorithms used for constellation recovery, we also describe a newly proposed DSP algorithm for distortion mitigation in a coherent receiver using single-ended photodetection.

## Reference


[1] Seb J. Savory, "Digital filters for coherent optical receivers," Optics Express, Vol 16, No. 2, pp. 804-817

[2] B. Spinnler, "Recent advances on polarization multiplexing," ECOC2008, paper TuD2.3

[3] Han Sun, Kuang-Tsan Wu, and Kim Roberts, "Real-time measurements of a 40 Gb/s coherent System," Optics Express, Vol. 16, No. 2, pp. 873-879, 2008.

[4] N. Kikuchi, K. Mandai, K. Sekine and S. Sasaki, "Incoherent 32-Level Optical Multilevel, Signaling Technologies" J. Lightwave Technolog, Vol. 26, No. 1, 2008.

[5] M. G. Taylor, "Coherent detection method using DSP for demodulation of signal and subsequent equalization of propagation impairments," *IEEE Photon. Technol. Lett.*, vol. 16, no. 2, Feb. 2004

[6] R. Noe, "PLL-free synchronous QPSK polarization multiplex/diversity receiver concept with digital I&Q baseband processing," *IEEE Photon. Technol. Lett.*, vol. 17, no. 4, pp. 887-889, Apr. 2005.

[7] S. Tsukamoto, D.-S. Ly-Gagnon, K. Katoh, K. Kikuchi, "Coherent demodulation of 40-Gbit/s polarization-multiplexed QPSK signals with 16-GHz spacing after 200-km transmission," Proc. OFC 2005, paper PDP-29.

[8] C. R. S. Fludger, T. Duthel, D. Van den Borne, C. Schulien, E. D. Schmidt, T. Wuth, E. De Man, G. D. Khoe, H. de Waardt, "10×111 Gb/s, 50 GHz spaced, POLMUX-RZ- DQPSK transmission over 2375 employing coherent equalization,' *Proc.OFC2007*, Anaheim, CA, 2007, PDP 22.

[9] G. Charlet, J. Renaudier, H. Mardoyan, P. Tran, O. B. Pardo, F. Verluise, M Achouche, A. Boutin, F. Blache, J. Dupuy, S. Bigo, "Transmission of 16.4 Tbit/s Capacity over 2550km using PDM QPSK modulation format and coherent receiver, " *Proc.OFC2008*, San Diego CA, 2008, PDP3.

[10] X. Zhou, J. Yu, D. Qian, T. Wang, G. Zhang, P. Magil, "8x114Gb/s, 25-GHz-spaced, polmux-RZ-8PSK transmission over 640km of SSMF employing digital coherent detection and EDFA-only amplification," in: OFC 2008, 2008, PDP1

[11] J. Yu, X. Zhou, D. Qian, M. F. Huang, P. N. Ji, G. Zhang, "20×112Gbit/s, 50GHz Spaced, PolMux-RZ-QPSK Straight-line Transmission over 1540km of SSMF Employing Digital Coherent Detection and pure EDFA Amplification," in: ECOC 2008, 2008, paper Th.2.A.2.

[12] J. Yu, X. Zhou, M. F. Huang, Y. Shao, D. Qian, T. Wang, M. Cvijetic, P. Magill, L. Nelson, M. Birk, S. Ten, H. B. Matthew, S. K. Mishra, "17 Tb/s (161×114 Gb/s) PolMux-RZ-8PSK Transmission over 662 km of Ultra-low Loss Fiber using C-band EDFA Amplification and Digital Coherent Detection," in: ECOC 2008, 2008, PDP Th.3.E.2

[13] X. Zhou, J. Yu, D, Qian, "A novel DSP algorithm for improving the performance of digital coherent receiver using single-ended photo detection," in ECOC 2008, 2008, paper Mo.4.D.1.

[14] X. Zhou, J. Yu and P. D. Magill, "Cascaded two-modulus algorithm for blind polarization de-multiplexing of 114-Gb/s PDM-8-QAM optical signals," OFC 2009, paper OWG3

[15] J. Yu, X. Zhou, M. F. Huang , D. Qian, L. Xu, and P. N. Ji, "Transmission of hybrid 112 and 44 Gb/s PolMux-QPSK in 25 GHz channel spacing over 1600 km SSMF employing digital coherent detection and EDFA-only amplification," OFC 2009, paper OThR3

[16] A. Leven, "Frequency estimation in intradyne reception," *IEEE Photon.. Technol. Lett.*, vol. 19, no. 6, Mar. 15, 2007

[17] D. N. Godard, "Self-recovering equalization and carrier tracking in two-dimentional data communication systems," IEEE Trans. Communications, Vol. Com-28, Nov. 11, 1980, pp. 1867-1875.

[18] A. J. Viterbi and A. M. Viterbi, "Nonlinear estimation of PSK-modulated carrier phase with application to burst digital transmission," *IEEE Trans. Inf. Theory*, vol. IT-29, no. 4, Jul. 1983.

[19] J. G. Proakis, *Digital Communications*, Fourth edition, Chapter 6

[20] Louchet, K. Kuzmin, A. Richter, "Improved algorithm for coherent 16QAM transmission," ECOC'08, TU.1.E.6, 2008.